AIAA 2002-0302

Transition Research in the Boeing/AFOSR Mach-6 Quiet Tunnel

Steven P. Schneider, Craig Skoch, Shann Rufer,
Shin Matsumura, and Erick Swanson
School of Aeronautics and Astronautics
Purdue University
West Lafayette, IN 47907-1282 USA

40th Aerospace Sciences Meeting & Exhibit
14–17 January 2002
Reno, Nevada

Transition Research in the Boeing/AFOSR Mach-6 Quiet Tunnel

Steven P. Schneider,* Craig Skoch,† Shann Rufer,‡ Shin Matsumura,§ and Erick Swanson.¶
School of Aeronautics and Astronautics
Purdue University
West Lafayette, IN 47907-1282

Abstract

A 9.5-inch Mach-6 Ludwieg tube is being developed for quiet-flow operation to high Reynolds number. Fluctuations in the bleed slot are thought to be tripping the nozzle-wall boundary layer and causing the noisy flow presently observed. Mean flow and fluctuation measurements are reported for five different bleed-slot geometries; all result in noisy flow even at the lowest Reynolds numbers presently achievable. Mean pitot profiles show good flow uniformity and cold-wire measurements yield temperatures near the expected values. Temperature-sensitive paints and an automated probe traverse are also being developed. Progress is summarized and future plans are indicated.

Introduction

Hypersonic Laminar-Turbulent Transition

Laminar-turbulent transition in hypersonic boundary layers is important for prediction and control of heat transfer, skin friction, and other boundary layer properties. However, the mechanisms leading to transition are still poorly understood, even in low-noise environments. Applications hindered by this lack of understanding include reusable launch vehicles such as the X-33 [1], high-speed interceptor missiles [2], hypersonic cruise vehicles [3], and ballistic reentry vehicles [4].

Many transition experiments have been carried out in conventional ground-testing facilities over the past 50 years. However, these experiments are contaminated by the high levels of noise that radiate from the turbulent boundary layers normally present on the wind tunnel walls [5]. These noise levels, typically 0.5-1% of the mean, are an order of magnitude larger than those observed in flight [6, 7]. These high noise levels can cause transition to occur an order of magnitude earlier than in flight [5, 7]. In addition, the mechanisms of transition operational in small-disturbance environments can be changed or bypassed altogether in high-noise environments; these changes in the mechanisms change the parametric trends in transition [6].

For example, linear instability theory suggests that the transition Reynolds number on a 5 degree half-angle cone should be 0.7 of that on a flat plate, but noisy tunnel data showed that the cone transition Reynolds number was about twice the flat plate result. Only when quiet tunnel results were obtained was the theory verified [8]. This is critical, since design usually involves consideration of the trend in transition when a parameter is varied. Clearly, transition measurements in conventional ground-test facilities are generally not reliable predictors of flight performance.

Development of Quiet-Flow Wind Tunnels

Only in the last two decades have low-noise supersonic wind tunnels been developed [5, 9]. This development has been difficult, since the test-section wall boundary-layers must be kept laminar in order to avoid high levels of eddy-Mach-wave acoustic radiation from the normally-present turbulent boundary layers. A Mach 3.5 tunnel was the first to be successfully developed at NASA Langley [10]. Langley then developed a Mach 6 quiet nozzle, which was used as a starting point for the new Purdue nozzle [11]. Unfortunately, this nozzle was removed from service due to a space conflict. Langley also attempted to develop a Mach 8 quiet tunnel [9]; however, the high temperatures required to reach

*Associate Professor. Associate Fellow, AIAA.
†Research Assistant. Student Member, AIAA.
‡Research Assistant. Student Member, AIAA.
§Research Assistant. Student Member, AIAA.
¶Research Assistant. Student Member, AIAA.

Mach 8 made this a very difficult and expensive effort. This tunnel was officially shut down in early 2001; quiet flow was not achieved and prospects for eventual success were judged poor (Steve Wilkinson, private communication, 2000). The new Purdue Mach-6 quiet flow Ludwieg tube may be the only operational hypersonic quiet tunnel in the world, at least until the old Langley Mach-6 nozzle is brought back online.

Background of the Boeing/AFOSR Mach-6 Quiet Tunnel

A Mach-4 Ludwieg tube was constructed at Purdue in 1992. By early 1994, quiet-flow operation was demonstrated at the low Reynolds number of about 400,000 [12]. Since then, this facility has been used for development of instrumentation and for measurements of instability waves under quiet-flow conditions (e.g., Ref. [13, 14, 15]). However, the low quiet Reynolds number imposes severe limitations; for example, the growth of instability waves under controlled conditions on a cone at angle of attack was only about a factor of 2 [16]. This is far smaller than the factor of $e^9 - e^{11}$ typically observed prior to transition, and small enough to make quantitative comparisons to computations very difficult.

A hypersonic facility that remains quiet to higher Reynolds numbers was therefore needed. The low operating costs of the Mach-4 tunnel had to be maintained. Operation at Mach 6 was selected, since this is high enough for the hypersonic 2nd-mode instability to be dominant under cold-wall conditions, and high enough to observe hypersonic roughness-insensitivity effects, yet low enough that the required stagnation temperatures do not add dramatically to cost and difficulty of operation. References [17] and [18] describe the overall design of the facility, and the detailed aerodynamic design of the contraction and quiet-flow nozzle.

Reference [19] reports on design and testing of some of the component parts, including the driver-tube heating, the as-measured contraction contour, the throat-region mandrel fabrication and polishing experience, and so on. Ref. [20] reports on the design and fabrication of the support structure, diffuser, second-throat section, and contraction. Ref. [20] also reports on the vacuum system, and on the contour measurements on the third attempt at throat-mandrel fabrication. Ref. [21] reports on the nozzle fabrication, the contraction-region heating apparatus, the burst-diaphragm tests, the bleed-slot suction system, and the electroformed throat properties. Ref. [22] reports the rest of the measurements of the as-fabricated nozzle, and included initial measurements of tunnel performance. The present tunnel name was adopted in Spring 2001. The present paper reports on progress toward achieving and characterizing uniform quiet flow.

The Boeing/AFOSR Mach-6 Quiet Tunnel

Quiet facilities require low levels of noise in the inviscid flow entering the nozzle through the throat, and laminar boundary layers on the nozzle walls. These features make the noise level in quiet facilities an order of magnitude lower than in conventional facilities. To reach these low noise levels in an affordable way, the Purdue facility has been designed as a Ludwieg tube [12]. A Ludwieg tube is a long pipe with a converging-diverging nozzle on the end, from which flow exits into the nozzle, test section, and second throat (Figure 1). A diaphragm is placed downstream of the test section. When the diaphragm bursts, an expansion wave travels upstream through the test section into the driver tube. Since the flow in the prototype Mach-4 tube remains quiet after the wave reflects from the contraction, sufficient vacuum can extend the useful runtime to many cycles of expansion-wave reflection, during which the pressure drops quasi-statically. The low operating cost of about $10/shot includes maintenance of the pumps and heaters, but does not include models, instrumentation, or the labor of the single graduate student needed to operate the facility.

Figure 2 shows the nozzle of the new facility. The region of useful quiet flow lies between the characteristics marking the onset of uniform flow, and the characteristics marking the upstream boundary of acoustic radiation from the onset of turbulence in the nozzle-wall boundary layer. A 7.5-deg. sharp cone is also drawn on the figure. The cone is drawn at the largest size for which it is likely to start [23, 24]. The uniform-flow region is drawn for the design condition with laminar nozzle-wall boundary layers. The locations of the two pitot traverses carried out so far are also shown.

Probe Traversing Mechanism

A mechanism has been designed to traverse probes through the test area of the nozzle. Axial motion is controlled manually, with movement being performed between runs. However, vertical movement is controlled automatically, permitting movement during a run. This should allow obtaining a full boundary-layer profile within a single run.

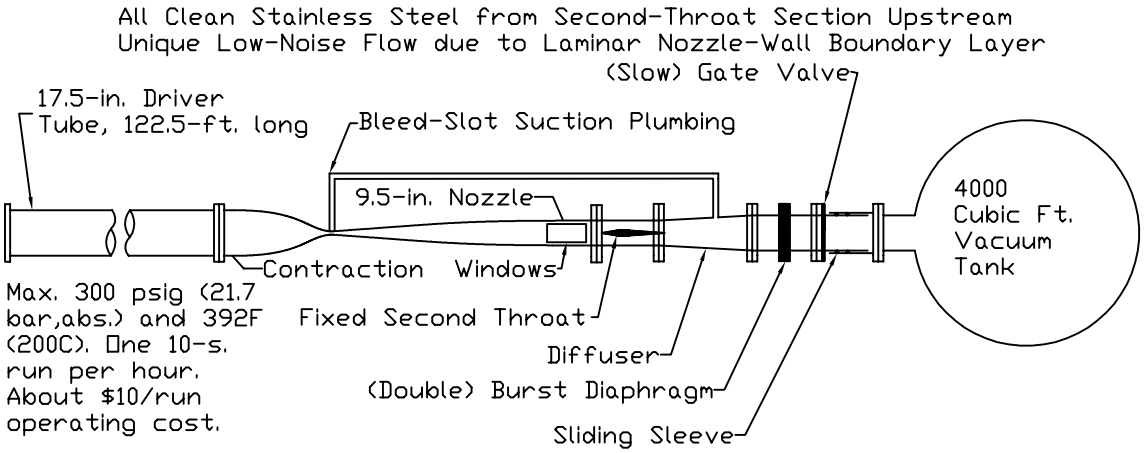

Figure 1: Schematic of Boeing/AFOSR Mach-6 Quiet Tunnel

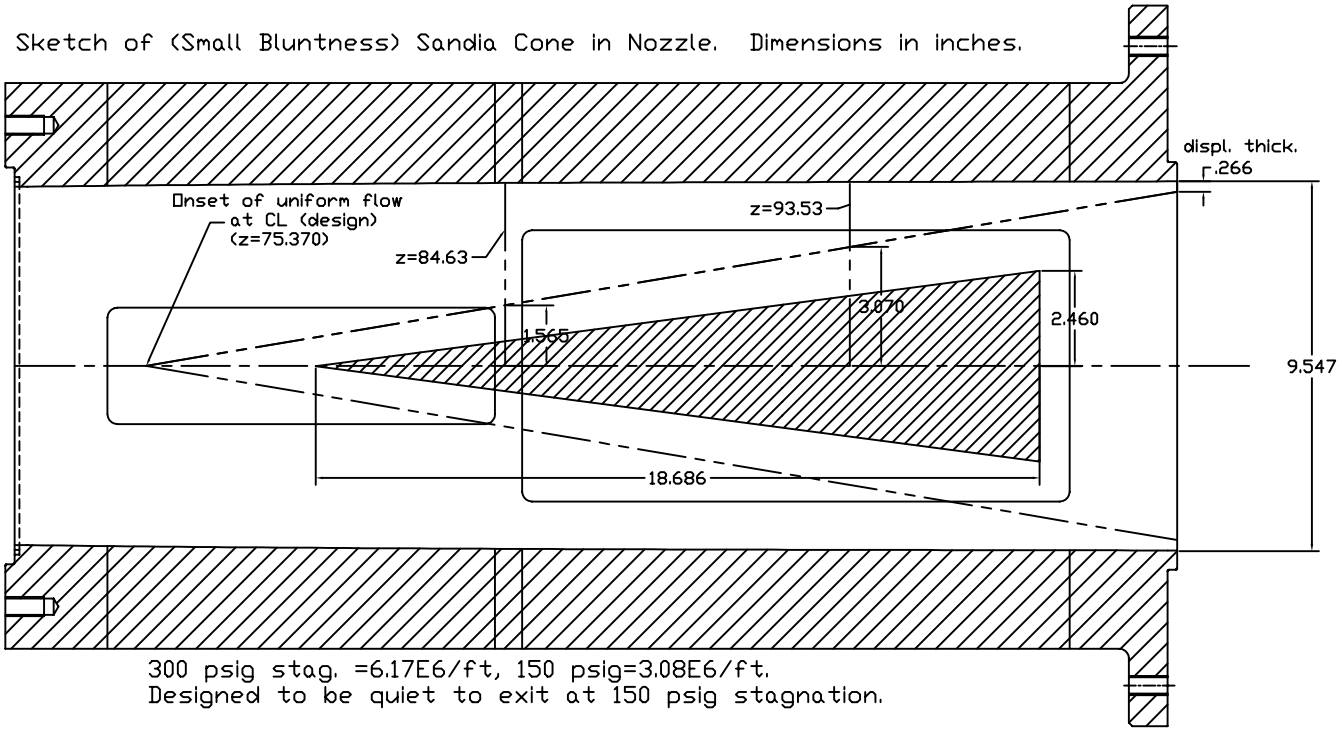

Figure 2: Schematic of Mach-6 Quiet Nozzle with Model

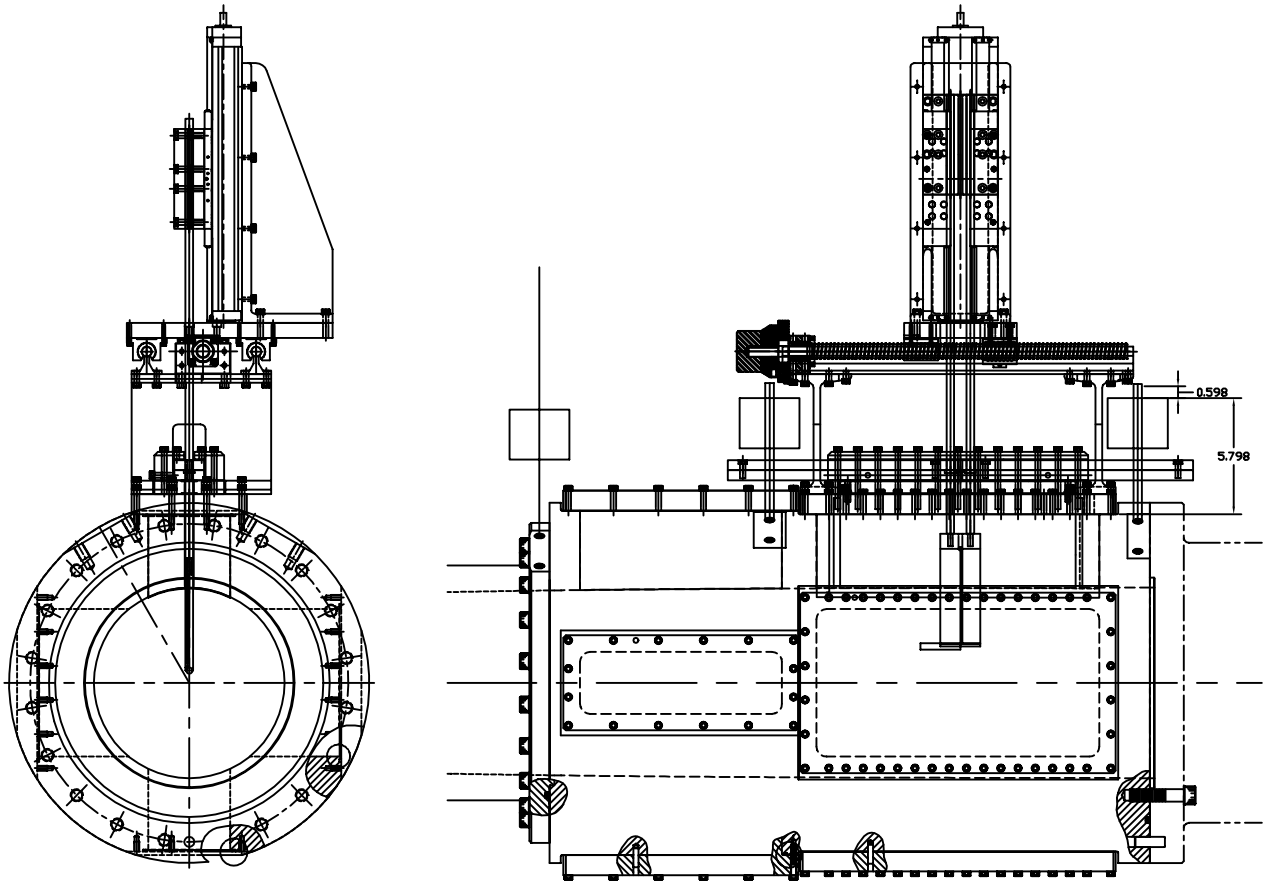

Figure 3: Schematic of Probe Traverse Mounted in Nozzle. Dimensions in Inches.

Fig. 3 shows the traverse, which has two parts: an upper part that supports the Parker stepper motor (not shown) and the Parker linear positioner, and a lower part consisting of two rails mounted on support struts that are bolted to the tunnel. Linear bearings allow the upper section to slide along the rails in the axial direction. This motion is actuated by a drive screw attached to the rearmost support strut and the bottom of the upper assembly.

Two probe support rods extend from the probe holder out of the test section through a slotted window blank and capping plate. An O-ring provides a seal between the plate and window blank. The top sections of the support rods are clamped to the linear positioner. A third, smaller rod conveys probe wiring out of the tunnel. This rod extends upward between the two larger support rods. The three rods pass through two bronze bars above the plate that are held in place by clamping blocks. The rods slide through holes in each bronze bar, sealed by O-rings. Screws in the clamping blocks can be loosened to allow the bronze bars to slide over the plate as the traverse moves in the axial direction. After moving the traverse, the screws are re-tightened to compress another O-ring between the bars and plate, to seal the tunnel.

The stepper motor is controlled by a Parker Gemini GT6 Stepper Controller. The motor system is designed for minimal electrical noise. Parker Compumotor Motion Planner software, running on a PC, is used to communicate with the controller. Control commands can be sent to the controller individually or as part of an uploaded program. The controller accepts commands detailing the distance, velocity, acceleration, and deceleration of each step move. A time delay before each move can also be specified.

The stepper motor and its control system have been tested and are now operational in either manual or programmed-control mode. A Fortran program accepts the parameters for each experimental run and translates them into a control program for Motion Planner. The Fortran program asks the user to input the number of step motions and the distance,

velocity, acceleration, deceleration, and time delay of each individual step. These values will be determined for each experiment to allow enough time at each location to take a measurement. At present, execution of control programs is initiated by command from the PC. In the future, these programs will be triggered from one of the pressure transducers in the tunnel. Program execution will begin as the pressure drops at the beginning of the tunnel run. A feedback loop in which an encoder measures the travel of the linear positioner and conveys this information to the computer will be developed. This will provide an independent measurement of the location of the probe in the tunnel and will potentially allow for on-the-fly motion adjustments. The positioning of the probe by the traverse system will be verified by looking through the window in the test section with a telescope and reticle.

Some problems were found during initial operations. The probe support rods have been binding up in the bronze bars, probably due to friction with the O-rings, and bending of the bars. Therefore, a new system is being designed that will include self-aligning linear bearings to guide the probe support rods. External seals designed for use with the bearings will most likely be used to seal the rod passages. New bronze bars must be designed to support the bearings and the external seals. These modifications are still in the conceptual stage.

Mean Flow and Noise Measurements

These measurements were carried out using techniques similar to those described in Refs. [22] and [25]. The data were acquired using LeCroy 9304AM and 9314AL oscilloscopes, sampling 8 bits at rates from 10-500 kHz, depending on the purpose. The Kulite transducers were connected to custom-built electronics, which supplied 10.00V from AD587 IC's and amplified the output using INA103 IC's. The DC output was first amplified by a factor of 100 for a DC output; this output was then high-pass filtered at 800 Hz and again amplified by a factor of 100 for a low-noise high-frequency output that resolves very small fluctuations. Similar electronics was used for a 2.5 mA constant-current anemometer for the cold-wire measurements.

The Kulite pressure transducers are compensated to limit temperature effects to within 1% of full scale for a 100F change. Many measurements are, however, carried out at pressures that are much less than full scale, since the tunnel can operate at driver-tube pressures from 300 psia to 14 psia or less. Since the pitot sensors in the nozzle begin a run at room temperature, and are heated by the flow during the run by an uncertain amount, the uncertainty in the temperature compensation dominates present uncertainties in pressure measurements. For example, calibrations of a slot-throat Kulite at 170C and 25C yield parallel lines offset by about 1.67 psia or 2.5% at about 68 psia. For measurements at lower pressures this error becomes much larger. Although transducers were generally calibrated at temperatures approximating those present during a run, corrections for these temperature variations have not yet been attempted. Kulite transducers with built-in sensing of the diaphragm temperature are available and are to be used in the future to reduce this uncertainty.

Timing

Ref. [22] discusses the timing of the pressure signals from the suction plenum, bleed slot, and test-region pitot pressure. Unfortunately, there was an error in the timing of Fig. 32 in Ref. [22]; the two traces in that figure came from different oscilloscopes with different trigger settings, so an error was made when the two traces were placed on the same time-base.

Fig. 4 shows a new and correct plot of the relative timing of the three signals. The run was for a driver-tube pressure of 1 atm. and a driver-tube temperature of $170°C$. The pitot signal, P_{t2}, was for a transducer located at $z = 84.31 \pm 1/16$ in., within 1/16 in. of the centerline (see Fig. 2). Here, z is an axial coordinate along the nozzle centerline, where $z = 0$ at the nozzle throat, and $t = 0$ when the expansion fan passes the pitot Kulite, triggering the oscilloscope. The pressure near the throat of the bleed slot is P_{th}, and the pressure in the plenum of the suction-slot system is P_{pl}. As in Figs. 24 and 25 of Ref. [22], the pitot pressure drops about 7 ms before the slot-throat pressure starts to drop. The initial drop in the slot-throat pressure is caused by reversed flow from the suction plenum into the contraction. At about 0.023 s, the suction plenum pressure starts to drop, and about 5 ms later the slot-throat pressure drops again, presumably establishing forward flow through the suction slot.

The slot-throat pressure stabilizes at about 0.04 s, and the pitot pressure appears nearly constant at about 0.04-0.06 s, but the suction plenum pressure is still dropping. Fig. 5 shows the same data, but plotted over a 1-s interval. Although the pitot pressure stabilizes in less than 0.25 s, it takes about 0.5

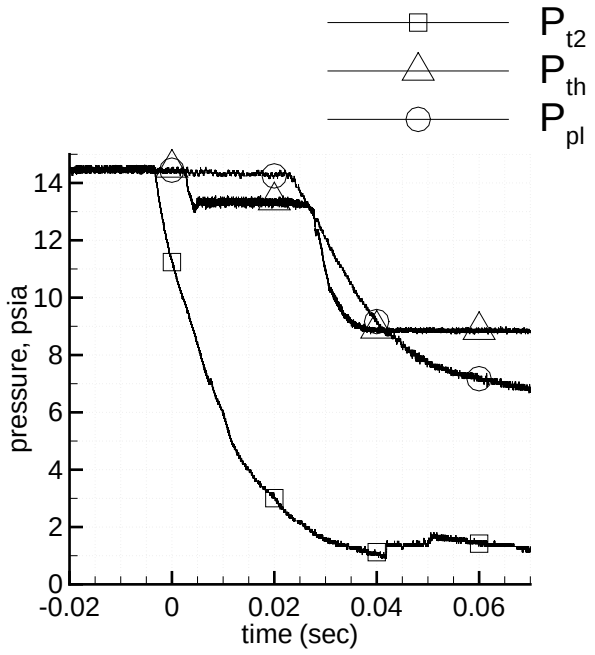

Figure 4: Sample Startup Timing, Case 1

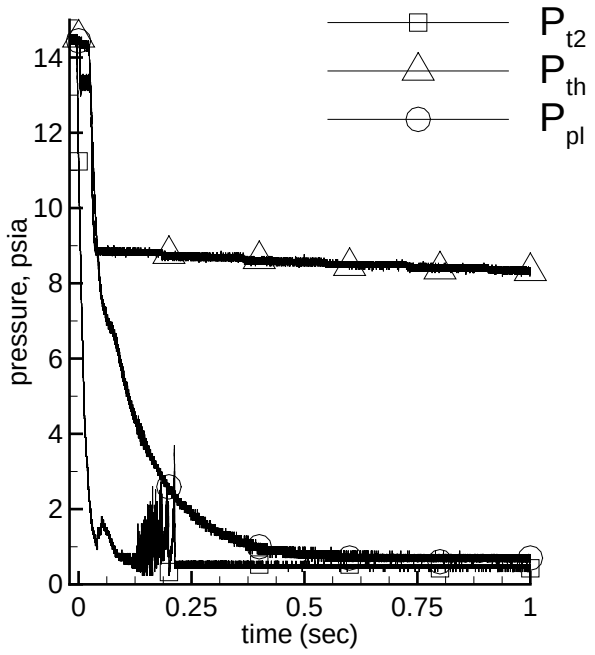

Figure 5: Sample Startup Timing: Longer Trace

s for the slot-suction plenum to reach its minimum value.

A Kulite XCE-080-250A pressure transducer was also placed flush with the contraction wall near the entrance to the contraction, at $z = -34.47$ in. It was installed primarily to determine the pressure fluctuations in the driver tube. However, a trace of the mean pressure is shown in Fig. 6. The initial driver-tube pressure was 131.06 psia, and the initial temperature was $90°C$. The data were sampled at 100 kHz. Fifty points have been averaged into each central point presented here. The figure shows stairstep drops in the pressure, as the expansion wave passes the sensor. Nine steps can be observed in 1.78 s, for an interval of 0.20 sec. The pressure drops about 1 psia per step, or about 0.8%. At $90°C$, the speed of sound in air is about 381 m/s, so the expansion wave travels about 76.2 m between drops. In one round-trip of the expansion wave, it passes through the driver tube twice, and reflects at some unknown effective position somewhere inside the contraction. The effective length of the driver-tube plus contraction is therefore 38.1 m. This corresponds nicely to the length of the driver tube (122.5 ft. or 37.34 m) and the contraction (40 in. or 1.02 m), indicating that the wave reflects about 3/4 of the way into the very gradual contraction. Presumably the stairsteps could also be measured in the pitot pressure in the nozzle, but records with sufficiently high resolution have not yet been obtained. The results appear very similar to those obtained earlier in the Mach-4 tube [26].

Throat-Region Bleed-Slot Geometries

As discussed in Ref. [22], problems with fluctuations in the bleed-slot throat are the primary suspect for the cause of the lack of quiet flow. Three different mechanisms seem feasible: (1) fluctuations in the massflow through the slot, which fluctuate the stagnation point on the bleed lip, and induce oscillations in the nozzle-wall boundary layer, (2) a separation bubble on the main-flow side of the bleed lip, due to a stagnation point located on the suction side of the lip, which again fluctuates and induces oscillations in the nozzle-wall boundary layer, and (3) insufficient suction through the bleed slot, which allows unsteadiness in the upstream contraction-wall boundary layer to propagate downstream past the lip into the nozzle-wall boundary layer.

The planned NASA Langley Mach-18 quiet tunnel also seemed to have problems with the bleed slot [9, pp. 5-6]. The Mach-3 'quiet' tunnel at ONERA in France is also not yet running quiet; the cause is believed to be problems with the bleed-slot geometry. Ref. [27] shows visualizations of a simulated bleed-slot flow in a water channel. These show that separation bubbles can occur on the main-flow side

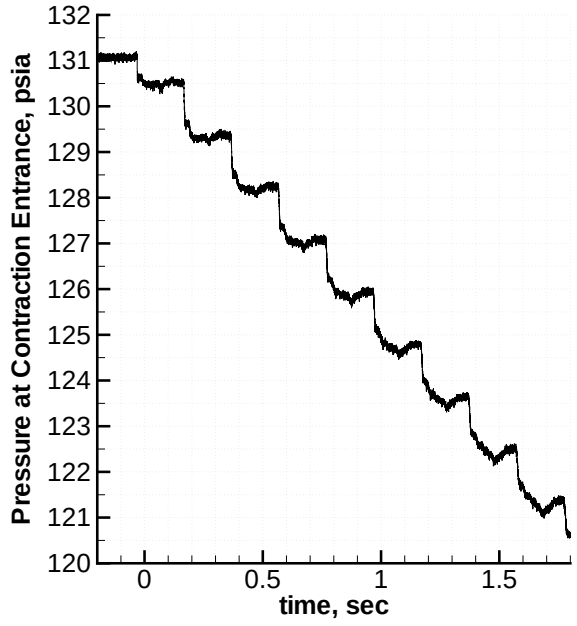

Figure 6: Pressure Trace at Contraction Entrance, Case 4

No.	Case	'entry', in.	'min.', in.
1	Original	0.036	0.029
2	Truncated Ring	0.036	0.029
3	No Ring	0.036	0.036
4	Brass Ring	0.073	0.042
5	Brass, 2nd Cut	0.073	0.062

Table 1: Bleed-Slot Geometries Tested

of the bleed lip if the slot massflow or lip positioning is not good. Such separations are likely to be unsteady, and to lead to early transition on the wall of the nozzle. Ref. [28] shows Navier-Stokes computations of the flow in the bleed slot of the ONERA 'quiet' tunnel. Again, separation bubbles are shown to be possible if the conditions are not right.

Table 1 lists the various bleed slot geometries tested. Fig. 7 shows the original bleed slot configuration (Cases 1-3). The original throat ring inserted into the end of the contraction, at the location shown, and formed the bleed slot, the inner surface of the slot being the outer surface of the nozzle lip. The outer surface of the nozzle lip is cylindrical, except for a 0.030-in.-diam. tip. Fig. 8 shows a detail of the slot itself. The height of the upper wall above the top of the tip is defined as 'entry', and the minimum height of the slot is defined as 'min.' These parameters are provided in Table 1 for all the

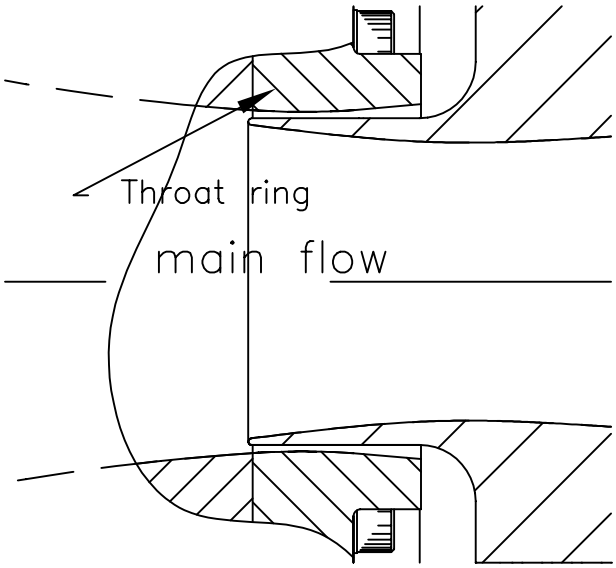

Figure 7: Original Bleed-Slot Configuration (Case 1)

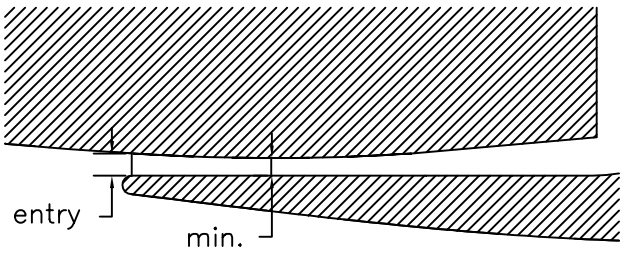

Figure 8: Detail Defining Critical Dimensions of Slot Throat

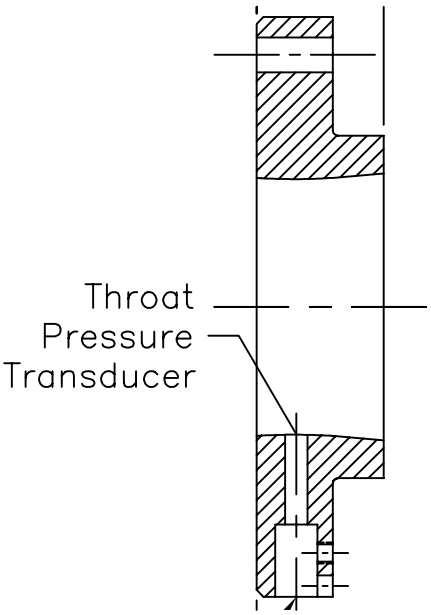

Figure 9: Original Throat Ring (Case 1)

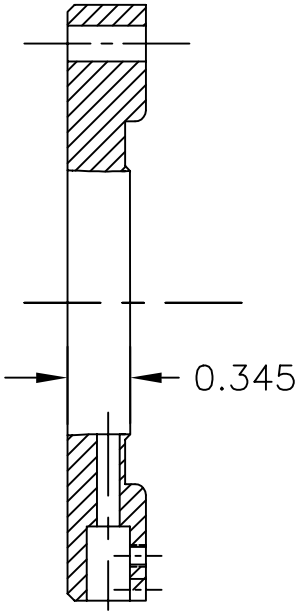

Figure 10: Truncated Throat Ring (Case 2). Dimension in Inches.

cases.

Fig. 9 shows the original throat ring (Case 1). The pressure transducer was located at the geometrical minimum of the slot. The upper surface of the slot was a circular arc. This 'Case 1' was the geometry used for the results presented in Refs. [22] and [25].

During the Anaheim AIAA meeting in June 2001, Profs. Garry Brown of Princeton and William Saric of ASU suggested that the problem with oscillations in the bleed-slot throat pressure might be due to an unsteady shock-boundary-layer interaction in the diverging section of the bleed slot, past the transducer. Both suggested removing this section, and terminating with a sharp edge. The idea was to fix the location of the sonic line at the edge, stopping any oscillations in the massflow. Supersonic flow should still exist in the expansion fan around the sharp edge, precluding any upstream influence of the noise present in the slot-suction plumbing. This geometry was first implemented by truncating the throat ring (Fig. 10). The original slot configuration (Fig. 7) and this new throat ring (Fig. 10) form Case 2 for the slot geometry.

The next attempt was to increase the massflow through the slot. Unfortunately, this could only be done to a limited extent, since the original throat ring was too small. For Case 3, the original throat ring was removed completely, leaving a sharp edge termination of the upper side of the slot, immediately behind the 0.030-diam. tip of the bleed lip (Fig. 7 with the throat ring removed).

It then became apparent that it was necessary to increase the amount of massflow through the slot, and probably also to increase the capture area of the slot. The original slot design called for 10% of the incoming massflow to be sucked through the slot [18]. Although this seemed sufficient, it was far less than the 30% used by Beckwith et al. for the Langley Mach-8 design [29, p. 6], and the 20-30% recommended in Ref. [30, p. 8]. To achieve these increases, a new contour was needed for the end of the contraction, which was much easier to change than the outside face of the bleed lip.

The code used to design the original contour (Ref. [18]) was therefore modified to allow a smooth variation in the contour of the end of the contraction. A third region of the contraction was added, wherein a new cubic was used to define the contour. This region started at a match point (here at $z' = 37.0$ in.), where the radius and its first derivative were matched. Here, z' is a coordinate along the contraction centerline, with $z' = 0$ at the entrance to the contraction. At the end of the new section of the contraction, a new and slightly larger radius is chosen, but the slope is maintained the same as in the original contraction, so the streamlines coming into the bleed lip still have about the same angle, which is approximately midway between the angles of the top and bottom of the bleed lip. The new contour is shown in Fig. 11, along with the original contour

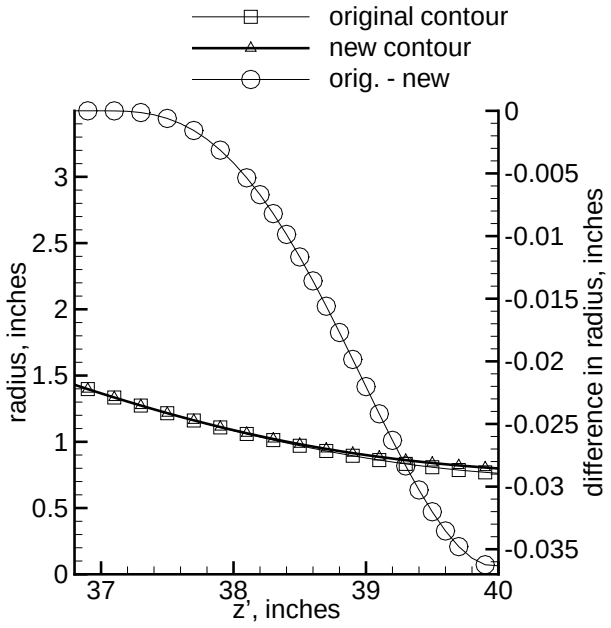

Figure 11: Modified Contraction Contour

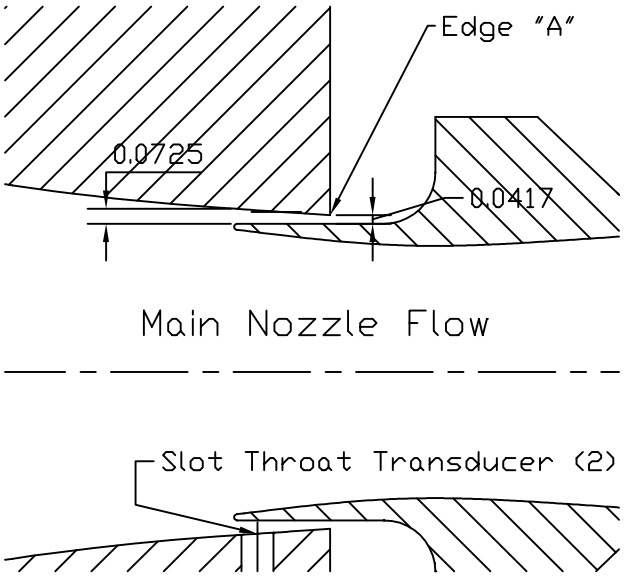

Figure 12: Bleed-Slot Configuration 4. Dimensions in Inches.

and the difference between the two. It can be seen that only a very small change is needed to double the height of the slot at the entrance. In the new design, a conical contour was maintained past the entrance to the slot. This conical contour could be cut short to increase the minimum slot height, keeping the sharp downstream edge now thought desirable. The axisymmetric panel code was again exercised for the new design (see Ref. [18]); it again appeared that good flow could be obtained if the correct slot massflow was achieved.

The last section of the contraction was bored out for the new and larger throat-ring insert, and the new insert was fabricated from brass. Fig. 12 shows configuration 4, the first using the new insert. For this insert, two Kulites were inserted in the slot throat, at the same axial location, but separated 135 deg. in azimuth to check the symmetry of the flow.

To increase the massflow through the slot of this new brass insert, the minimum could be machined back, as was done for configuration 5, shown in Fig. 13. This is nearly the largest massflow that could be achieved without moving the throat pressure transducer.

For the first brass throat ring geometry, measurements were made with the two transducers in the throat. The results are shown in Fig. 14. The two traces show almost exactly the same timing. The initial pressures are identical and equal to the

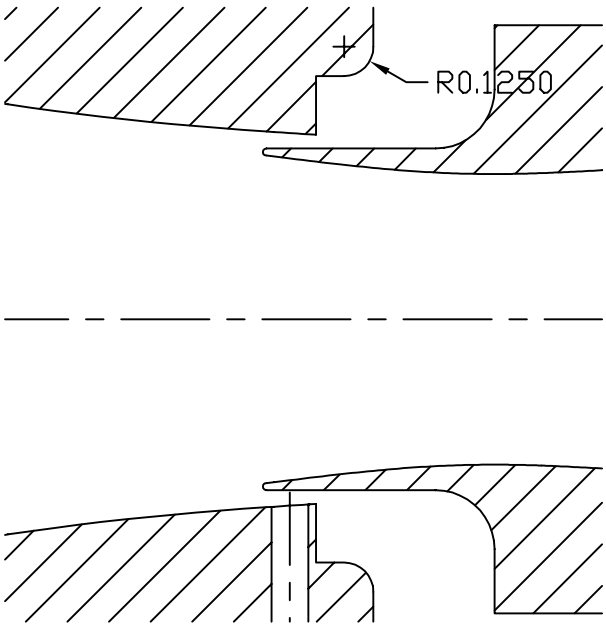

Figure 13: Bleed-Slot Configuration 5. Dimension in Inches.

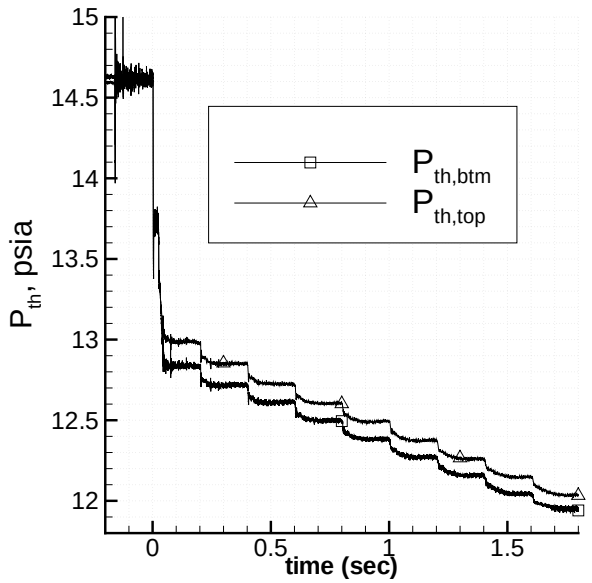

Figure 14: Pressure Traces at Bleed-Slot Throat, Case 4

initial driver-tube pressure, but the pressures shown during the run differ by about 0.15 psia, or about 1.2%. This difference appears to be somewhat larger than the error in the calibration. It may be due to small flaws in the pressure-tap hole, small differences in the location of the transducer within the hole, or small asymmetries in the slot flow. The stairsteps in the figure are similar to those shown in Fig. 6.

Measurements on Centerline for Various Conditions

Pitot measurements were carried out on the centerline of the tunnel ($\pm$ 1/16 in.), with the probe full forward on the traverse. The case 1 data were obtained at $z = 84.3 \pm 1/16$ in. The data for cases 2-4 were obtained at $z = 84.63 \pm 1/16$ in. The Case-5 data were obtained at $z = 84.16 \pm 1/16$ in. The data were sampled at 500kHz by 8-bit LeCroy digital oscilloscopes. The bleed-slot valves were open for all runs, which thus had slot suction.

A number of different datasets were accumulated to test various effects. These are listed in Table 2. The names in the table are used to identify the datasets in the figures. For 'Rufer 1', the temperature of the air filling the driver tube was varied, to determine whether an effect was observed. For 'Rufer 2', the humidity of the driver-tube air was varied, by partially filling the tube with humid air from the room, before filling with dry air from

Name	Case	Comments
Rufer 1	1	Varied Circ. Heater Temp.
Rufer 2	1	Varied Humidity
Rufer 3	1	Cold Contraction
Rufer 4	1	Normal Procedure
Skoch 1	1	Early Runs, Humidity Present
Case 2	2	
Case 3	3	
Case 4	4	
Case 5	5	

Table 2: Sets of Pitot Measurements on Tunnel Centerline

the compressor plant. For 'Rufer 3', the contraction temperature was varied, which varies the temperature of the first air entering the nozzle. This could cause problems with the calibration of the throat Kulites, whose built-in temperature compensation may be insufficient to maintain full accuracy. For 'Rufer 4', normal procedures were used. The data labeled 'Skoch 1' was obtained for Ref. [25], using early procedures. In these early procedures, the driver-tube was vented up to atmospheric pressure after a run, using air bled in through the pressure regulator from the room. Thus, this air has some humidity in it. Funding has not yet permitted the acquisition of a dewpoint meter, so the driver-air dewpoint is not yet known.

The last 4 datasets were taken to evaluate Cases 2-5 of the bleed slot configurations. The first three of these were taken at a substantially lower driver-tube temperature, since failure of 1 of the 3 power supplies heating the driver tube precluded achieving a higher temperature.

Figure 15 shows the results for the RMS fluctuations of the pitot pressure, normalized by the mean. For quiet flow, a value less than about 0.1% should be achieved. The data are plotted against the initial driver-tube pressure, P_d, which is equal to the stagnation pressure. The initial driver-tube temperature is T_d. The data all show the noise level decreasing from 2-4% at 1 atm. to 0.5-1.5% at about 9 atm. This decrease of normalized noise with increasing unit Reynolds number is typical of conventional facilities with turbulent nozzle-wall boundary layers [6]. The data for Cases 1 and 5 fall together, with the data for Cases 2-4 falling at a significantly lower level. While it was thought that the changes in noise level were caused by the differences in the bleed-slot geometry and the corresponding changes in nozzle-wall boundary layer, they may also be caused by the

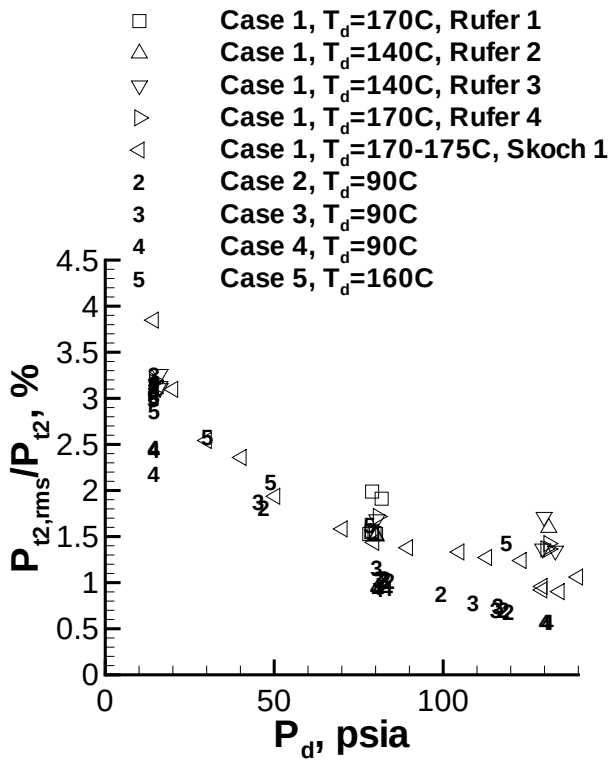

Figure 15: Pitot Fluctuations on Centerline

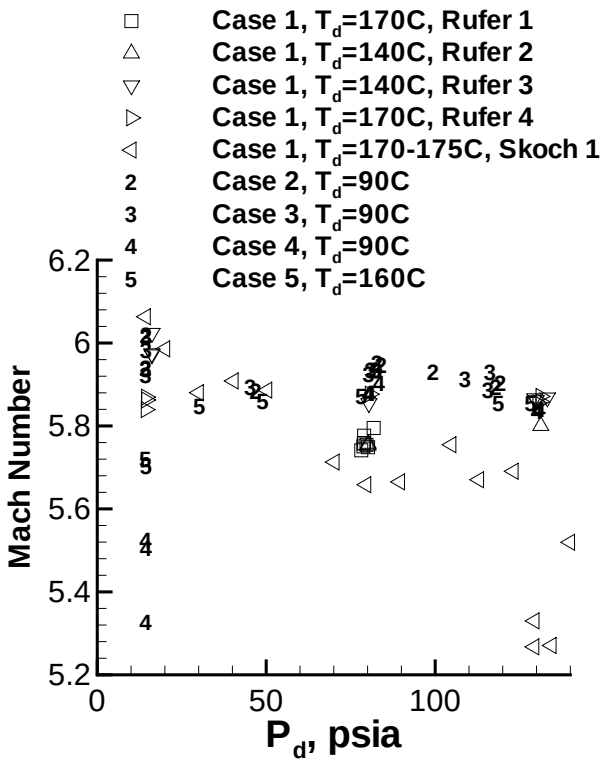

Figure 16: Mach Number on Centerline

changes in stagnation temperature. This possibility is currently being investigated.

Fig. 16 shows the corresponding measurements of Mach number, obtained using the Rayleigh pitot formula from the mean pitot pressure and the driver-tube pressure. Most of the data show Mach numbers between 5.8 and 6.0. Only some of the variations can at present be explained. The Mach number data reported in Ref. [22] are incorrect; they are about 3% low due to an error in the algorithm that reduced the pitot-pressure data to Mach number.

The 'Skoch 1' data is somewhat below the other data, perhaps because of excessive humidity in the supply air. The four data points with Mach numbers between 5.2 and 5.6 at $P_d \simeq 140$ psia were among the first taken in Spring 2001, and probably suffer from humidity problems. Wegener et al. (Ref. [31, p. 438]) states that *'...the pitot pressure with condensation is always greater than in the absence of condensation, except immediately behind the condensation shock.'* Thus, if we neglect the possibility of the condensation shock immediately in front of the sensor, the measured Mach number will be lowered by the presence of condensation. Except for the 'Skoch 1' and 'Rufer 2' data, all the runs were obtained using only air drawn through the compressor and dryer. However, the dewpoint of the air cannot at present be measured, as stated earlier. The 'Rufer 2' data were taken later, with differing amounts of room air drawn into the driver tube, to vary humidity. These runs show almost no effect of humidity. In view of the lack of dewpoint data, the cause must remain unknown.

Carl Peterson from Sandia National Laboratory has suggested that perhaps condensation occurred in the early humid runs, due to residual dust in the system, while no condensation may have occurred in later runs, if the dust was successfully removed, so that nucleation sites for condensation were no longer present. Table 3 shows results from two runs that were made to check condensation effects. Both of these measurements were made with some humidity present in the driver tube, from the tube initially being bled up to 1 atm. from room air. These runs were made with the Case 1 configuration. One of the two runs was made with a stagnation temperature which should be above condensation values, and shows fairly typical results for Mach number and pitot fluctuations. The other run was made with a room-temperature driver tube, which should cause

P_d, psia	T_d	Mach No.	$P_{t2,rms}/P_{t2}$
79.49	24C	5.73	0.41%
70.33	170C	5.68	1.54%

Table 3: Pitot Measurements on Nozzle Centerline at $z = 84.305$ in.

condensation, yet the mean Mach number for this data shows almost no change, while the pitot fluctuations drop by a factor of more than 3 to the lowest value yet seen. Since this run was made after the tunnel had been operated for some time, Peterson's hypothesis may hold true – it is the only explanation that so far seems feasible. The low pitot fluctuations for the low-stagnation-temperature case may be caused by changes in the nozzle-wall turbulent boundary layer due to the temperature.

The other curious data in Fig. 16 are the low Mach numbers measured only at $P_d = 1$ atm. for Cases 4 and 5. Since Case 4 has a larger intercept area for the bleed lip, and a small minimum for the suction slot, one might suspect separation from the lip. However, one would expect this to reduce the massflow through the nozzle throat, and thus increase the Mach number. The cause of this variation is at present unknown. Aside from this, there is no clear effect of the bleed-slot geometry on the mean Mach number; any effect is within the scatter.

Fig. 17 shows the mean pressure on the transducer in the bleed-slot throat, normalized by the driver pressure. No data is shown for Case 3, since there was no throat transducer. The ratio is closest to the sonic value, 0.528, for Case 2. This is not surprising, since the transducer is at the geometrical minimum, and there is very little duct downstream of this location. However, the Case 2 values of 0.55-0.58 are slightly but significantly above 0.53, indicating that the flow area is still contracting at the geometrical minimum.

For Case 1, the ratio is significantly subsonic, increasing slightly with increasing driver pressure. Since the boundary layers would be thinner at higher pressure, the cause of the increase is unknown. For Case 4, the ratio is very high. Based on the area ratio of $1.57 = 0.066/0.042$ between the transducer and the minimum, the Mach number at the transducer should be about 0.41, and $P_{th}/P_d \simeq 0.89$, which is just above the measured value of 0.86-0.88. This suggests that viscous effects are minimal. This throat pressure decreases for Case 5, as would be expected given the increased massflow associated with the increase in minimum height. For Case 5, the area ratio

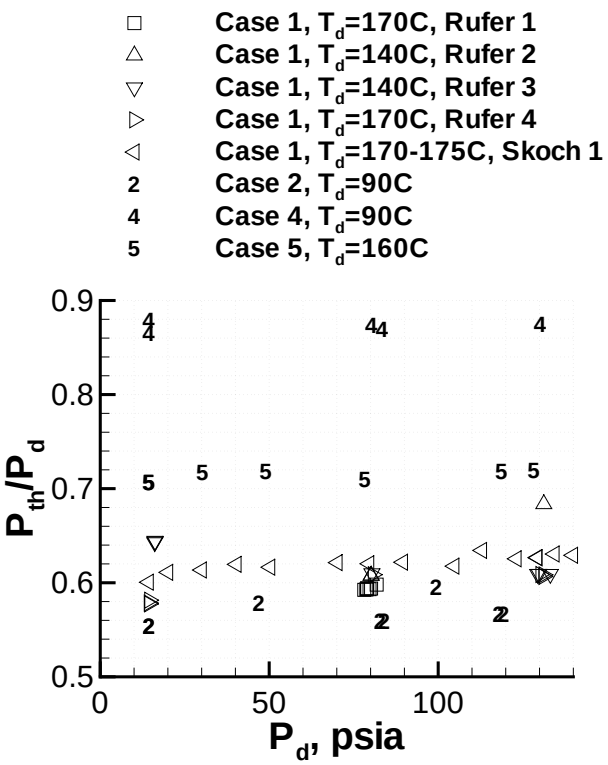

Figure 17: Mean Pressure in Bleed-Slot Throat

to the transducer from the minimum would yield a Mach number of about 0.75 at the transducer, for $P_{th}/P_d \simeq 0.69$, which is just below the measured value of 0.70-0.72, again suggesting minimal viscous effects.

The Mach number at the bleed-lip tip on the main-flow side of the lip is about 0.66, using a simple one-dimensional analysis, like that used by Beckwith [32]. This yields $P/P_d \simeq 0.75$ just past the tip of the lip, on the main-flow side. Again, if the pressures are not well matched on the two sides of the bleed-lip tip (where direct measurements are not thought feasible), then flow around the tip may cause disturbances that trip the nozzle-wall boundary layer. Using Table 1 and assuming inviscid isentropic flow between the 'entry' and 'min.', and neglecting any effects of the 0.030-in. lip tip, one can obtain Table 4. Here, A/A^* is the area ratio between the slot entry and the slot minimum, and P/P_d is the local one-dimensional pressure divided by the total pressure (assumed equal to P_d.) For all but Case 3, the pressures at the slot entrance may be too high, and may be driving flow around the tip into a separation bubble on the main-flow side.

Fig. 18 shows the results for the RMS fluctu-

Case No.	A/A^*	P/P_d
1,2	0.56	0.81
3	1.00	0.53
4	1.73	0.91
5	1.18	0.78

Table 4: Isentropic One-Dimensional Slot-Entry Pressures

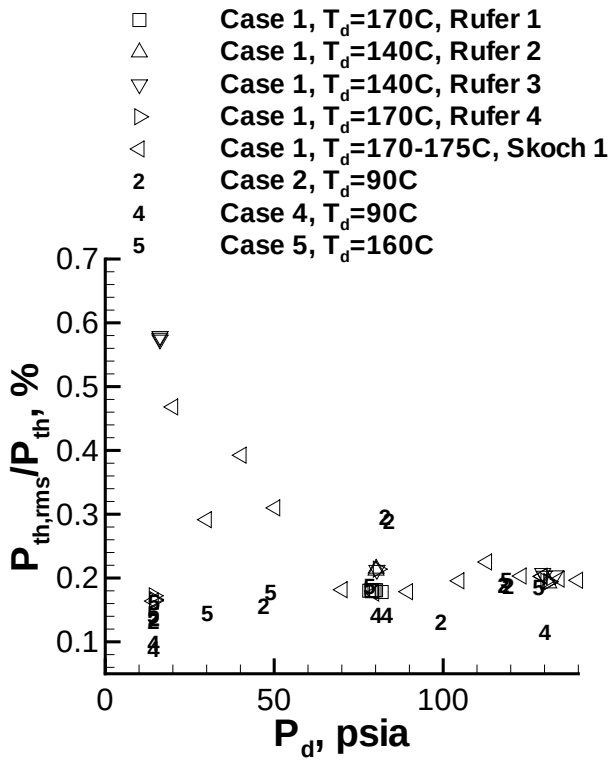

Figure 18: Fluctuations in Bleed-Slot Throat

ations on the transducer in the bleed-slot throat. The RMS is divided by the mean value. The values for Case 1 range from about 0.2% at high pressure, to 0.15-0.6% at low pressure. Although the 'Skoch 1' values generally increase with decreasing pressure, both the Skoch and Rufer datasets show some very low values at $P_d = 1$ atm., and some much higher values at slightly higher driver pressures. This jump is repeatable, and remains a mystery. The signal/noise ratio for this data is substantial at the higher pressures (roughly 10-20), decreasing to near 1 for the 0.15% results at 1 atm.

The fluctuations for Case 2 with the truncated ring are generally somewhat lower, except near 85 psia. They never show the high values found at low pressures for Case 1. Case 4 has the lowest fluctu-

P_d, psia	T_d,C	P_{ce}, psia	$P_{ce,rms}/P_{ce}$
131.1	90	129.3	0.010%
80.8	90	79.8	0.016%
14.6	90	14.4	0.088%

Table 5: Pressure Near Contraction Entrance

ations, while Case 5 is somewhat higher. The signal/noise ratio for Case 5 varies almost linearly from about 2 at $P_d = 15$ psia to about 20 at $P_d = 130$ psia.

Thus, substantial fluctuations still exist in the subsonic region of the bleed slot, at least at moderate and high pressures. The cause of these fluctuations is unknown. Do these fluctuations arise upstream, or do they only occur in the slot throat?

To answer this question, a transducer was installed near the entrance to the contraction, at $z = -34.47$ in., to measure the mean and fluctuations where the diameter is still nearly the same as the driver-tube diameter. The data were averaged over a time period 0.25-0.35 s after flow initiation. Table 5 shows the results to date. The pressure near the contraction entrance (P_{ce}) is slightly lower than the driver tube pressure, possibly because of pressure drops between the initial setting and the time at which the signal was averaged, or possibly due to transducer calibration errors. The difference also bounds the error caused by assuming the driver tube pressure is the upstream stagnation pressure (and neglecting the effect of the expansion wave).

The fluctuation levels at the higher pressures are extremely small, rising at the lower pressure as the signal level decreases. The signal/noise ratio was computed using the transducer noise from before the run began, which is thought to be caused primarily by electronic noise. For all three datapoints this is 1.0, indicating that the pressure fluctuations during the run do not rise above the pre-run values. Since these fluctuation levels are much smaller than in the bleed-slot throat, it is believed that fluctuations are developing in the suction region of the throat. These may be causing fluctuations in the early part of the nozzle-wall boundary layer, inducing early transition there.

Finally, there was initially some concern about having sufficient suction to provide sonic flow at the minimum of the bleed slot. A transducer was added to the plenum that exists just downstream of the bleed slots. Fig. 19 shows the measurements for the mean pressure in this plenum. The data were averaged over a period from 1.3 to 1.8 s. after flow

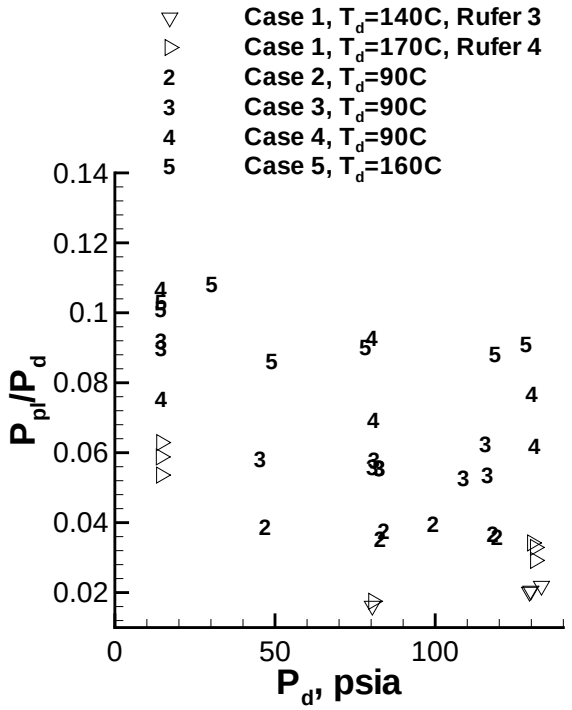

Figure 19: Mean Pressure in Suction Plenum for Bleed Slot

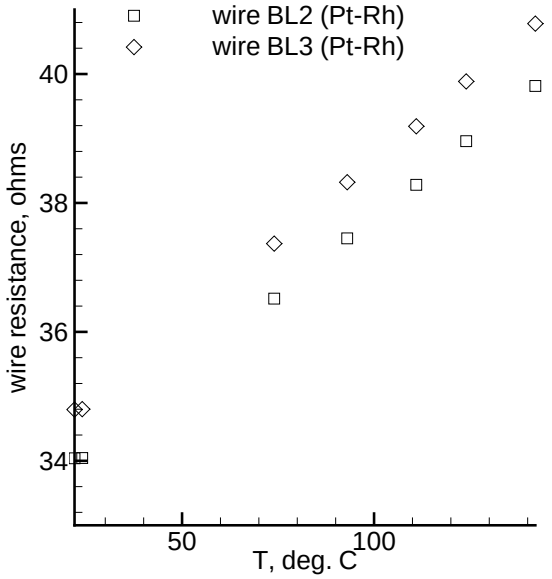

Figure 20: Oven Calibrations of Cold Wires

initiation. Although this is rather late in the run, the plenum data drop slowly (Fig. 5). If the Case 5 data were averaged from 0.6 to 1.1 s, the results are only about 4% higher.

For Case 1, with the small slot minimum, and the extended downstream channel, the pressure is lowest, as might be expected, since the massflow appears smallest. For Case 2, with the truncated throat ring, the massflow is higher, since the pressure at the slot transducer is lower (see Fig. 17). The plenum pressure thus increases. For Case 3, the minimum height is again higher, and the massflow again increases, increasing the plenum pressure. For Case 4, with double the entry height, and an increased slot minimum, the pressure increases again. For Case 5, with a substantially increased minimum, the pressure scatters less, but seems to be about the same, on the high end of the Case 4 data, although the minimum height is increased by 50% from Case 4. It is not clear why the plenum pressure does not rise more between cases 4 and 5. All the pressures are small compared to the sonic value, suggesting there is plenty of suction to establish sonic flow at the minimum in the bleed slot.

Cold-Wire Measurements of Stagnation Temperature

Cold wire measurements were made to determine the stagnation temperature in the nozzle. Only four runs have been made so far, all with the Case 4 configuration. Most of the runs were made with Pt-10%Rh wires, 0.0001 inches in diameter, which are welded to needles that have a tip diameter of 0.003 inches. A small amount of bow is included in the wire. The wires were calibrated in an oven. A sample calibration is shown for the Pt-Rh wires in Fig. 20. The slopes are nearly identical for the two wires of identical material, as would be expected, and the last point, taken at room temperature, nearly repeats the first point.

The wires were placed on the tunnel centerline in the uniform flow region at about $z = 89$ in. The data were sampled at 50kHz. The sampled data were averaged over running intervals of 11 points to reduce the high frequency noise. Figure 21 shows the results for the temperature measurements. The wire temperature, T_w, is inferred from the voltage and the oven calibration. It is normalized by the driver-tube temperature, T_d. For $t < 0$, the flow has not begun yet, but the wire temperature is not equal to the driver temperature; this is expected because only the driver tube and contraction are heated, while the downstream end of the nozzle remains near room temperature. All the runs were made at a driver

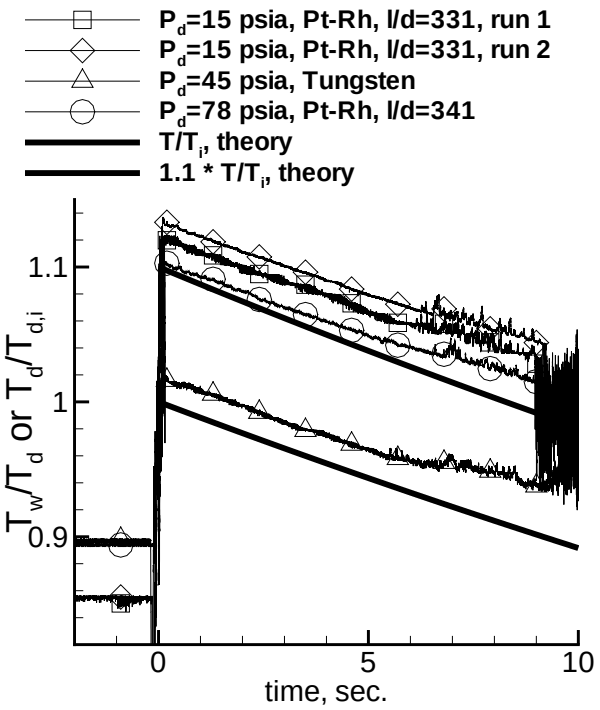

Figure 21: Cold-Wire Measurements of Temperature

temperature of 363K.

The first two runs, at $P_d = 15$ psia, both show a nearly equal initial temperature of 312K, or about 39C, somewhat above room temperature. The latter two runs, at higher tunnel pressure, show an initial temperature of about 327K, or about 54C. This is probably because hot air is blown through the driver tube to pressurize the nozzle and driver tube, for runs above 1 atm. total pressure, and the nozzle air remains above room temperature when the run begins.

The temperature fluctuates widely during the tunnel startup, near $t = 0$ sec., and then reaches a peak in the initial Mach-6 flow. It then drops slowly as the flow expands out of the driver tube, as in the Mach-4 Ludwieg tube [33]. The first two runs use the same wire, and start from the same conditions, producing peak values of T_w/T_d that repeat closely near 1.11. For these conditions, the Mach number is about 5.8, the wire Reynolds number is about 0.6 and the Knudsen number is about 2.1 (computed using the mean-free-path formula (eqn. 1-32) from Ref. [34]). In this region, the recovery factor is dependent on Mach number [35]. No data is shown in Refs. [35] or [36] for these conditions, although the nearest data suggests a recovery factor of about 1.10-1.14. This agrees pretty well with the present results, neglecting any effects of conduction into the wire supports. However, the computation of mean free path used by Ref. [36] differs substantially from that of Ref. [34], so correlations to the literature remain uncertain. The present wire operating conditions are very similar to those used by Dewey (Refs. [37] and [38]); however, his data-reduction methods have not yet been implemented, and comparisons to his results remain to be obtained.

The run at 45 psia with the tungsten wire produces a much smaller peak temperature, for unknown reasons. The diameter of the tungsten wire is either 0.0001 or 0.00015 inches, and the length is 0.026 inches. The run with the Pt-Rh wire at 78 psia produces a slightly lower temperature, possibly because the wire Reynolds number is slightly higher, reducing the recovery factor. The three wires all broke after one or two runs, usually during tunnel shutdown. The long-term survivability of reasonable wire configurations remains to be determined.

A theoretical trace for the driver temperature as a function of time is also shown. This theory is based on the temperature drop in the driver tube due to isentropic expansion of the gas, as described in Ref. [13]. The wire temperature drops at approximately the same rate as the expected drop in driver-tube temperature, suggesting that there is no marked change in recovery factor during the run, and that there are no marked effects of conduction to the wire supports. The theoretical trace was also multiplied by 1.1 to show a nearby comparison against the results with higher wire temperature. This shows that the wire temperature does not drop quite as fast as expected from the theory, especially after about $t = 5$ sec.; the cause of the different rate is as yet unknown. Fig. 6 in Ref. [13] shows good agreement with the isentropic theory for the Mach-4 Ludwieg tube, while Fig. 5 in Ref. [13] also shows the wire temperature dropping more slowly than the theory; the cause of that difference was never resolved. Overall, these early results show no problems with nonuniformities in driver-tube temperature, unlike the early results with the Mach-4 tube [39].

Profiles at Full-Forward Traverse Location

Fig. 22 shows the pitot profiles obtained at the full-forward location on the traverse, with the probe support all the way forward in the slot. The pitot Kulite is at $z = 84.63$ in., and the driver tube temperature was $90°C$ for all the runs. All the profiles were obtained with the truncated ring and the original bleed-slot geometry, case 2. The mean pitot

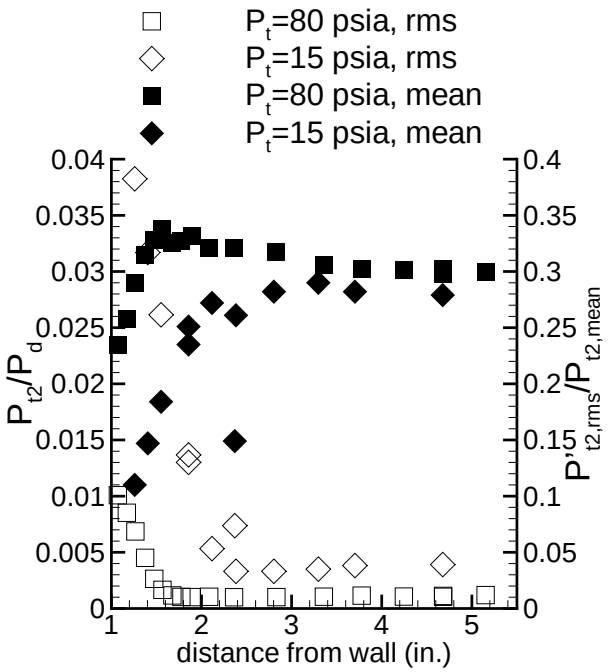

Figure 22: Pitot Profiles at $z = 84.63$ in.

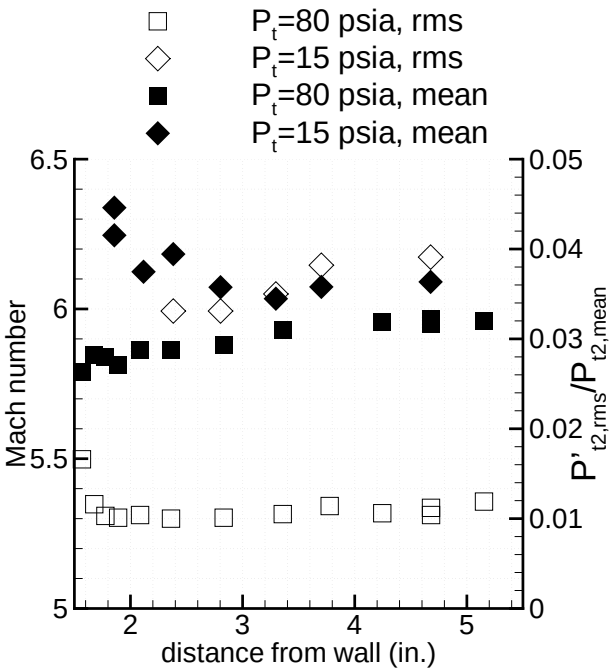

Figure 23: Core-Flow Profiles at $z = 84.63$ in.

pressure, P_{t2}, is shown normalized by the driver tube pressure, P_d. The plot also shows the rms pitot pressure, $P_{t2,rms}$, normalized by the mean pitot pressure. Both types of data are shown for two different driver pressures, 14.4 ± 0.2 psia and 80 ± 0.5 psia. The data were acquired on the 8-bit scopes at 500kHz. The mean was averaged over the period from 0.25-0.35 s after flow startup, and the RMS was obtained by averaging the AC part of the signal, from 0.25 to 1.75 s after flow startup. The horizontal coordinate is the distance from the wall at this location; the nozzle radius at this location is 4.722 inches, so the centerline is at 4.722 on this axis. Each data point was obtained in a separate tunnel shot. In addition, the data was obtained using random variations in the probe position, so the consistency in the data reflects shot-to-shot repeatability as well as the smooth profiles that apparently exist.

The square symbols show the results at a total pressure of 80 psia. The boundary layer is about 1.6 inches thick. Beyond this distance, the mean flow is fairly uniform, and the fluctuations fairly constant. The diamond symbols show the results for a total pressure of 15 psia. Here, the boundary layer is about 2-1/2 inches thick, with again fairly uniform conditions within the core. There is one flyer in the mean-flow measurements, which differs from the other data; the cause of this flyer is not yet known.

Fig. 23 shows a detail of the core portion of the flow, using the same data. The mean pitot measurements have been converted to mean Mach number profiles, using the Rayleigh pitot formula, which is valid outside the boundary layer. The driver tube pressure is assumed equal to the stagnation pressure, since the Mach number in the driver tube is only about 0.003, due to the large area ratio. The square symbols, for the 80 psia data, show that the mean Mach number varies from about 5.8, just outside the boundary layer, to about 5.95, near the centerline. The core flow here has a diameter of about 6.2 in. and a Mach number variation of about $\pm 1\%$. The rms pitot pressure for the 80 psia data is about 1%, which seems fairly typical for a 'conventional' tunnel with turbulent nozzle-wall boundary layers. The noise is fairly uniform across the core flow, as was reported by Laufer [40, p. 1193]. The diamond symbols, for the 15 psia data, show that the mean Mach number outside the boundary layer is between 6.0 and 6.1, and the pressure fluctuations in this region are a bit less than 4%. The core flow diameter is about 4-1/2 inches at this pressure. The mean Mach number is higher when the boundary layers are thicker at lower tunnel pressures, which is opposite to the usual behavior.

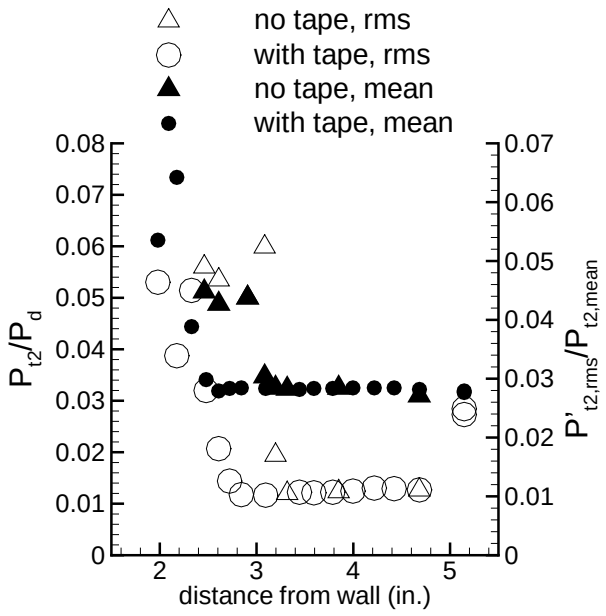

Figure 24: Pitot Profiles at $z = 93.53$ in.

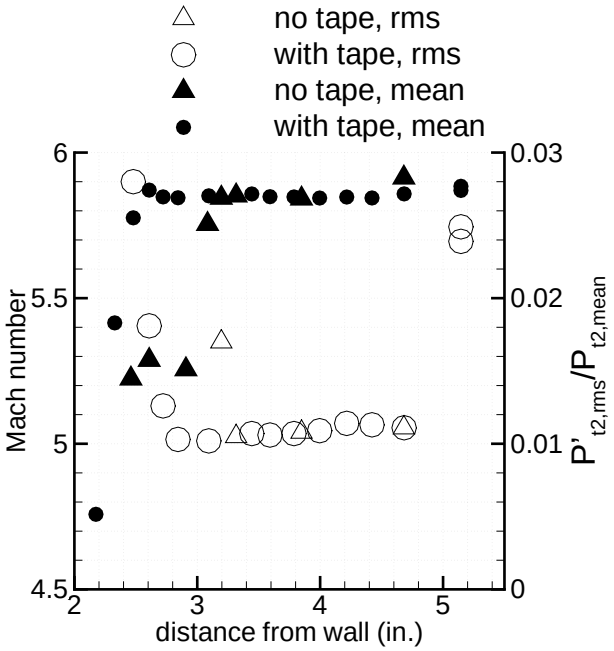

Figure 25: Core-Flow Profiles at $z = 93.53$ in.

Profiles at Full-Aft Measurement Location

Fig. 24 shows a second set of profiles obtained with the probe traverse full aft. For these runs, again carried out by randomly staggering the vertical probe position, the driver tube pressure was 80 psia and the driver-tube temperature was $90°C$. At this location, the radius of the nozzle is 4.749 in.

Two sets of data are shown in the figure. The triangular symbols show data obtained with the traverse slot open. This slot is 7/16-inch wide and extends about 9 inches in front of the probe. Since the slot is nearly 4 inches deep, the flow will stagnate in the depths of the slot, and a recirculation region will form, covered by a shear layer. The solid symbols show the mean-flow measurements. With the slot open, the higher near-wall pitot pressures extend to about 3 inches from the wall, and the higher near-wall rms pitot fluctuations extend to about 3-1/4 inches from the wall. The near-wall layer has thickened from about 1.6 inches (Fig. 22) to about 3-1/4 inches over a length of only 8.9 inches. It was thought that this was due to the effect of the recirculating flow over the traverse slot.

The slot was then covered with tape, in the region in front of the probe, and the measurements were repeated. The circular symbols in Fig. 24 show the results. The solid circles show that the mean pitot pressures drop to the core-flow values at about 2.6 inches from the wall, while the fluctuations drop to core values at about 2.8 inches from the wall. The boundary layer has still thickened from about 1.6 inches to about 2.6 inches over a length of only 9 inches, which seems remarkable. It is not clear whether the tape successfully removes all effects of the slot. Since the slot is present only in a blank window insert, it can be modified fairly easily or removed; however, the use of the traverse requires the slot.

Figure 25 shows a detail of the core region. The Mach number in the core region remains very near 5.75, with or without the tape. This is a 1-3% decrease from the 5.8 to 5.95 observed 9 inches upstream. With the tape, the core region starts at about 2.6 inches from the wall. This leaves a core diameter of 4.3 inches. The diameter of the core decreases from 6.2 inches to 4.3 inches over a length of only 9 inches, due to the boundary-layer growth. These values are much different from the design core diameters of 3.13 in. and 6.14 in. at the upstream and downstream stations (Fig. 2). The difference is presumably due to the presence of turbulent nozzle-wall boundary layers rather than the designed-for laminar layers. The nozzle is very long, so the variations in radius at the end are small, and the turbulent layer grows in a nearly constant pressure gradient. In the core region, the rms pitot fluctuations are about 1.1% of the mean. This seems to be a fairly

typical value for a facility with turbulent nozzle-wall boundary layers [6]. There are two higher values of the fluctuations at about 2%, just past the centerline; the reason for this repeatably higher value of the fluctuations is at present unknown.

Models

Progress in Fabrication of the Hyper2000 Model

The mechanisms of transition are to be studied on a generic scramjet-forebody geometry obtained from Charles McClinton at NASA Langley, which is called the Hyper2000. The centerline geometry on the forebody ramp appears to be the same as for the Hyper-X (X-43) [41]. This geometry is thought to be generic for a wide range of similar spatula-shaped airbreathing hypersonic cruise vehicles.

A model of the forebody of the Hyper2000 is being milled in the Aerospace Sciences Laboratory (ASL) at Purdue University for use in the Purdue Mach 6 Ludwieg Tube. The IGES files defining the geometry were translated into SDRC IDEAS, which was used in conjunction with SURFCAM to develop a CAM file for the 3-axis CNC mill. The Hyper2000 geometry was truncated at a position near where the combustor section would begin on the Hyper-X. The chines on the sides of the Hyper2000 model were cut to approximate the Hyper-X model tested by Berry [41], and to reduce the base area of the model so that a larger model could start in the wind tunnel. The final model will be 12 inches long and about 5.5 inches wide at the base. Two plastic models have already been built to test milling techniques. An aluminum model is to be fabricated by the ASL shop early in calendar year 2002.

Preliminary Measurements with Temperature-Sensitive Paints

Preliminary TSP experiments were performed on a nearly-sharp 7-deg. half-angle blockage cone model. A layer of Mylar tape was taped to the surface to minimize the heat transfer between the TSP layer and the model. The TSP used was Tris(2,2'- bipyridyl) dichloro-Ruthenium(II) hexahydrate, with DuPont's ChromaClear automotive paint as the binder. This particular TSP was chosen because it has good sensitivity in the expected temperature range [42], and because similar experiments were performed previously [43]. A blue LED was pulsed for 0.2 seconds to excite the paint. The fluorescence of the TSP was recorded using a 12-bit CCD camera.

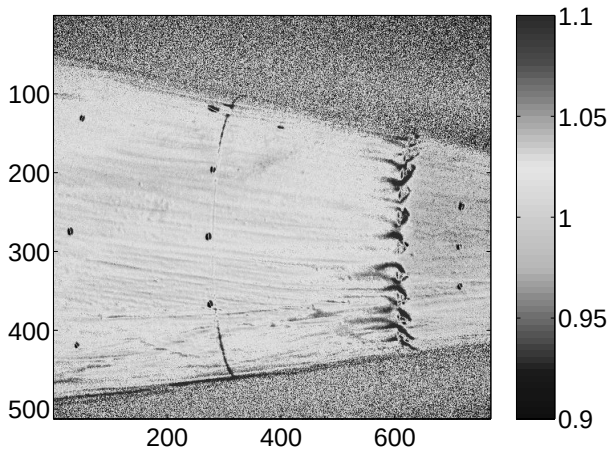

Figure 26: Temperature-Sensitive Paint Image of Cone

A sample result is shown in Figure 26. The scale is the ratio of the reference image, taken prior to the tunnel run, to the image taken during the run. This ratioing technique eliminates small nonuniformities in the paint and lighting. A calibration is usually done in these intensity-based methods to convert the ratio to actual temperatures. The horizontal and vertical scales on the figure are pixel counts; the scale has not been corrected to geometrical lengths. An array of roughness elements was glued to the model approximately 9.5 inches from the tip. The roughness elements were of triangular shape, with a height of 0.08 inches. Nine fiducial marks can also be seen as dark spots. The streamwise distance between the three furthest upstream and the three furthest downstream is 6.25 inches. The marks are required to correct the image for distortion from the curved window. The power series technique was used, but has not been successful for this model, so far [42]. Figure 26 thus has not been corrected.

However, the image does show that the overall temperature downstream of the roughness elements is higher, suggesting that the boundary layer is tripped. Bright streaky structures can also be seen downstream of the tips of the roughness elements. These may be streamwise vortices caused by the roughness. However, it is difficult to tell, since the paint was also brushed on in the streamwise direction, leaving streak marks. In later experiments the TSP will be sprayed onto the model.

Nonetheless the basic usefulness of the TSP technique has been verified, and work will continue to improve the techniques and the quality of the

images. Some models under consideration are the Hyper2000, blunt and sharp cones, and slab deltas. Other techniques for image correction will be investigated as well.

Blockage Tests

Several models have been constructed to perform blockage tests of the largest model that will start in the tunnel. Slab-delta models with a 70-deg. sweep have been tested, along with a nearly-sharp round cone. A pitot probe was used with the slab-delta models for initial tests, but these were inconclusive. High levels of fluctuations were sometimes observed with the pitot probe, which may be due to starting problems, or to interference between the model, traverse slot, and probe. A pressure transducer is to be mounted in the slab-delta models themselves, for further tests.

Summary and Future Plans

The Boeing/AFOSR Mach-6 quiet tunnel was completed in April 2001. Although low cost operation has been achieved, turbulent boundary layers are present on the nozzle walls to the minimum unit Reynolds number, so the tunnel noise level remains at conventional levels. Measurements of the fluctuations in the nozzle-throat bleed slot suggest that unsteadiness in the bleed-slot flow is tripping the nozzle-wall boundary layers. Five different bleed slot configurations have so far been tested, but none have yielded any quiet flow.

The pressure fluctuations in the entrance of the contraction are less than 0.1%, and the polish in the nozzle throat does not appear to be degrading during operation, suggesting that the air is very clean. Problems with the bleed slot thus remain the most likely cause of the complete lack of quiet flow. Tests with additional slot geometries are therefore planned. Measurements will also be carried out further upstream in the nozzle, to see if the wall boundary layer transitions near the uniform-flow region at low driver pressures.

In addition, a dewpoint meter is to be installed, and condensation effects are to examined. The probe traverse will be improved to allow obtaining mean-flow profiles within a single run. Temperature-sensitive paints are to be developed to examine transition on round-cone and Hyper2000 models. Hot-wire technique will be used for measurements of the mean flow and fluctuations in the boundary layers on these models.

The Mach number in the 4-6-inch-dia. core of the nozzle is about $5.8 \pm 2\%$. This permits initial experiments under conditions comparable to a conventional tunnel. Preliminary cold-wire measurements show that uniform temperatures are achieved in the driver tube. Instrumentation development and preliminary experiments can be carried out in the conventionally-noisy flow while work continues toward achieving quiet flow. Progress is to be reported in Ref. [44].

Acknowledgements

The research is funded by AFOSR under grant F49620-00-1-0016, monitored by John Schmisseur, by Sandia National Laboratory, under contract BG-7114, and by NASA Langley, under grant NAG1-01-027. The generous cooperation of Dr. Steve Wilkinson and the rest of the NASA Langley quiet tunnel group has been critical to our progress. Mr. Michael Rapp performed the detailed design of the traverse.

REFERENCES

[1] Scott A. Berry, Thomas J. Horvath, Brian R. Hollis, Richard A. Thompson, and H. Harris Hamilton II. X-33 hypersonic boundary layer transition. Paper 99-3560, AIAA, June 1999.

[2] H.A. Korejwo and M.S. Holden. Ground test facilities for aerothermal and aero-optical evaluation of hypersonic interceptors. Paper 92-1074, AIAA, February 1992.

[3] AGARD, editor. *Sustained Hypersonic Flight.* AGARD, April 1997. CP-600, vol. 3.

[4] Tony C. Lin, Wallis R. Grabowsky, and Kevin E. Yelmgren. The search for optimum configurations for re-entry vehicles. *J. of Spacecraft and Rockets*, 21(2):142–149, March-April 1984.

[5] I.E. Beckwith and C.G. Miller III. Aerothermodynamics and transition in high-speed wind tunnels at NASA Langley. *Annual Review of Fluid Mechanics*, 22:419–439, 1990.

[6] Steven P. Schneider. Effects of high-speed tunnel noise on laminar-turbulent transition. *Journal of Spacecraft and Rockets*, 38(3):323–333, May–June 2001.

[7] Steven P. Schneider. Flight data for boundary-layer transition at hypersonic and supersonic speeds. *Journal of Spacecraft and Rockets*, 36(1):8–20, 1999.

[8] F.-J. Chen, M.R. Malik, and I.E. Beckwith. Boundary-layer transition on a cone and flat plate at Mach 3.5. *AIAA Journal*, 27(6):687–693, 1989.

[9] S. P. Wilkinson, S. G. Anders, and F.-J. Chen. Status of Langley quiet flow facility developments. Paper 94-2498, AIAA, June 1994.

[10] I. Beckwith, T. Creel, F. Chen, and J. Kendall. Freestream noise and transition measurements on a cone in a Mach-3.5 pilot low-disturbance tunnel. Technical Paper 2180, NASA, 1983.

[11] Alan E. Blanchard, Jason T. Lachowicz, and Stephen P. Wilkinson. NASA Langley Mach 6 quiet wind-tunnel performance. *AIAA Journal*, 35(1):23–28, January 1997.

[12] S. P. Schneider and C. E. Haven. Quiet-flow Ludwieg tube for high-speed transition research. *AIAA Journal*, 33(4):688–693, April 1995.

[13] Steven P. Schneider, Steven H. Collicott, J.D. Schmisseur, Dale Ladoon, Laura A. Randall, Scott E. Munro, and T.R. Salyer. Laminar-turbulent transition research in the Purdue Mach-4 quiet-flow Ludwieg tube. Paper 96-2191, AIAA, June 1996.

[14] J.D. Schmisseur, Steven H. Collicott, and Steven P. Schneider. Laser-generated localized freestream perturbations in supersonic and hypersonic flows. *AIAA Journal*, 38(4):666–671, April 2000.

[15] Terry R. Salyer, Steven H. Collicott, and Steven P. Schneider. Feedback stabilized laser differential interferometry for supersonic blunt body receptivity experiments. Paper 2000-0416, AIAA, January 2000.

[16] Dale W. Ladoon and Steven P. Schneider. Measurements of controlled wave packets at Mach 4 on a cone at angle of attack. Paper 98-0436, AIAA, January 1998.

[17] Steven P. Schneider. Design of a Mach-6 quiet-flow wind-tunnel nozzle using the e**N method for transition estimation. Paper 98-0547, AIAA, January 1998.

[18] Steven P. Schneider. Design and fabrication of a 9-inch Mach-6 quiet-flow Ludwieg tube. Paper 98-2511, AIAA, June 1998.

[19] Steven P. Schneider. Fabrication and testing of the Purdue Mach-6 quiet-flow Ludwieg tube. Paper 2000-0295, AIAA, January 2000.

[20] Steven P. Schneider. Initial shakedown of the Purdue Mach-6 quiet-flow Ludwieg tube. Paper 2000-2592, AIAA, June 2000.

[21] Steven P. Schneider, Shann Rufer, Laura Randall, and Craig Skoch. Shakedown of the Purdue Mach-6 quiet-flow Ludwieg tube. Paper 2001-0457, AIAA, January 2001.

[22] Steven P. Schneider and Craig Skoch. Mean flow and noise measurements in the Purdue Mach-6 quiet-flow Ludwieg tube. Paper 2001-2778, AIAA, June 2001.

[23] D.A. Bountin, A.N. Shiplyuk, and A.A. Sidorenko. Experimental investigations of disturbance development in the hypersonic boundary layer on a conical model. In H. Fasel and W. Saric, editors, *Laminar-Turbulent Transition. Proceedings of the IUTAM Symposium, Sedona, 1999*, pages 475–480, Berlin, 2000. Springer-Verlag.

[24] C.J. Schueler. An investigation of model blockage for wind tunnels at Mach numbers 1.5 to 19.5. Technical Report AEDC-TN-59-165, Arnold Engineering Development Center, February 1960. DTIC citation AD-232492. Limited distribution.

[25] Craig Ryan Skoch. Final assembly and initial testing of the Purdue Mach-6 quiet-flow Ludwieg tube. Master's thesis, School of Aeronautics and Astronautics, Purdue University, December 2001.

[26] Steven P. Schneider, Christine E. Haven, Joseph B. McGuire, Steven H. Collicott, Dale Ladoon, and Laura A. Randall. High-speed laminar-turbulent transition research in the Purdue quiet-flow Ludwieg tube. Paper 94-2504, AIAA, June 1994.

[27] C. Quelin, S. Petit, and J. Delery. Etude au tunnel hydrodynamique TH1 du fonctionnement de la fente d'aspiration du collecteur de la soufflerie silencieuse R1Ch. Rapport Technique RT 1/03472 DMAE/DAFE, ONERA, Octobre 2000. In French.

[28] R. Benay, B. Chanetz, and B. Gheradi. Simulation numerique de l'ecoulement dans la tuyere de la soufflerie silencieuse R1Ch. Rapport Technique RT 2/05454 DMAE/DAFE, ONERA, Octobre 2001. In French.

[29] I. Beckwith, F. Chen, S. Wilkinson, M. Malik, and D. Tuttle. Design and operational features of low-disturbance wind tunnels at NASA Langley for Mach numbers from 3.5 to 18. Paper 90-1391, AIAA, June 1990.

[30] S.P. Wilkinson, S.G. Anders, F.-J. Chen, and I.E. Beckwith. Supersonic and hypersonic quiet tunnel technology at NASA Langley. Paper 92-3908, AIAA, July 1992.

[31] P.P. Wegener and L.M. Mack. Condensation in supersonic and hypersonic wind tunnels. *Advances in Applied Mechanics*, 5:307–447, 1958.

[32] Timothy Alcenius, S.P. Schneider, Ivan E. Beckwith, and John J. Korte. Development of square nozzles for high-speed low-disturbance wind tunnels. Paper 94-2578, AIAA, June 1994.

[33] Steven P. Schneider and Scott E. Munro. Effect of heating on quiet flow in a Mach 4 Ludwieg tube. *AIAA Journal*, 36(5):872–873, May 1998.

[34] F. M. White. *Viscous Fluid Flow.* McGraw-Hill Book Company, New York, 1992. Second edition.

[35] E.F. Spina and C.B. McGinley. Constant-temperature anemometry in hypersonic flow: Critical issues and sample results. *Experiments in Fluids*, 17:365–374, 1994.

[36] L.V. Baldwin, V.A. Sandborn, and J.C. Laurence. Heat transfer from transverse and yawed cylinders in continuum, slip, and free molecule air flows. *J. of Heat Transfer*, pages 77–86, May 1960.

[37] C. Forbes Dewey. Hot-wire measurements in low Reynolds number hypersonic flow. *ARS Journal*, pages 1709–1718, December 1961.

[38] C. Forbes Dewey. Hot-wire measurements in low Reynolds number hypersonic flow. Memorandum 63, Graduate Aero. Lab., California Inst. of Tech., Hypersonic Research Project, September 1961.

[39] Scott Edward Munro. Effects of elevated driver-tube temperature on the extent of quiet flow in the Purdue Ludwieg tube. Master's thesis, School of Aeronautics and Astronautics, Purdue University, December 1996. Available from the Defense Technical Information Center as AD-A315654.

[40] John Laufer. Some statistical properties of the pressure field radiated by a turbulent boundary layer. *Physics of Fluids*, 7(8):1191–1197, August 1964.

[41] Scott Berry, Aaron Auslender, Arthur D. Dilley, and John Calleja. Hypersonic boundary-layer trip development for Hyper-X. Paper 2000-4012, AIAA, August 2000.

[42] T. Liu, B.T. Campbell, S.P. Burns, and J.P. Sullivan. Temperature- and pressure-sensitive luminescent paints in aerodynamics. *Applied Mechanics Review*, 50(4):227–246, April 1997.

[43] S. Matsumura, C. Huang, Y.S. Choi, E.O. Swanson, T.R. Salyer, and H. Sakaue. Feasibility of detecting streamwise vortices from roughness elements using temperature sensitive paint in a Mach 4 Ludwieg tube. Winning Paper for 2001 AIAA GTTC Competition, 2001.

[44] Steven P. Schneider, Shin Matsumura, Shann Rufer, Craig Skoch, and Erick Swanson. Progress in the operation of the Boeing/AFOSR Mach-6 quiet tunnel. Paper 2002-XXXX, AIAA, June 2002. Submitted to the June 2002 AIAA Ground Testing Conference.